

Black holes in Einstein-aether and Hořava–Lifshitz gravity

Enrico Barausse¹, Ted Jacobson¹ and Thomas P. Sotiriou²

¹*Center for Fundamental Physics, University of Maryland, College Park, MD 20742-4111, USA*

²*Department of Applied Mathematics and Theoretical Physics, Centre for Mathematical Sciences, University of Cambridge, Wilberforce Road, CB3 0WA, Cambridge, UK*

(Dated: October 23, 2018)

We study spherical black-hole solutions in Einstein-aether theory, a Lorentz-violating gravitational theory consisting of General Relativity with a dynamical unit timelike vector (the “aether”) that defines a preferred timelike direction. These are also solutions to the infrared limit of Hořava–Lifshitz gravity. We explore parameter values of the two theories where all presently known experimental constraints are satisfied, and find that spherical black-hole solutions of the type expected to form by gravitational collapse exist for all those parameters. Outside the metric horizon, the deviations away from the Schwarzschild metric are typically no more than a few percent for most of the explored parameter regions, which makes them difficult to observe with electromagnetic probes, but in principle within reach of future gravitational-wave detectors. Remarkably, we find that the solutions possess a universal horizon, not far inside the metric horizon, that traps waves of any speed relative to the aether. A notion of black hole thus persists in these theories, even in the presence of arbitrarily high propagation speeds.

PACS numbers: 04.50.Kd, 04.70.Bw,

I. INTRODUCTION

Lorentz invariance is believed to be a fundamental symmetry of physical theories. Indeed, there are severe observational constraints on Lorentz-violating effects in the matter sector [1, 2]. On the other hand, in the much more weakly coupled gravitational sector such constraints are generically far weaker. Therefore, it is interesting to test Lorentz symmetry further in gravitational phenomena.

To do that in a well-defined way one must consider some candidate Lorentz-violating (LV) gravitational theory as a low energy effective theory. To violate Lorentz symmetry and still be manifestly diffeomorphism invariant, such a theory should include, apart from the metric, some dynamical field that can define a preferred frame at the level of the solution. A unit timelike vector field is an example which breaks local boost but not local rotation symmetries. The most general theory one can construct by coupling this field to general relativity (GR) at second order in derivatives is called Einstein-aether theory (\mathfrak{a} -theory) [3–5]. The vector field is referred to as the aether.

Apart from providing a test bed for constraining Lorentz violations in the gravitational sector, \mathfrak{a} -theory is an interesting theoretical laboratory to explore preferred frame effects without having to give up diffeomorphism invariance. Seen as a low energy effective field theory [6], it can be thought of as encapsulating LV effects that might arise in a more fundamental quantum gravity theory. Its viability as a low energy effective theory of gravity has been extensively tested against various different observations, and up to date there seems to be a significant portion of the parameter space for which the predictions agree with all current experimental evidence (see Ref. [5] for a review).

Recently, another proposal for a LV gravity theory has received a lot of attention, Hořava–Lifshitz (HL) gravity [7]. This is not supposed to be just an effective field theory. There is hope that it can constitute instead an actual UV completion of general relativity, as it appears to be power-counting renormalizable. This is achieved by adding higher order spatial derivatives, without adding higher order time derivatives, which lead to a suitable modification of the propagator. In HL gravity this involves the existence of a preferred spacelike foliation of spacetime, which is described by a scalar field.

The dynamics of this scalar (or the lack thereof) can lead to various problems in restricted versions of the theory such as instabilities, over-constrained evolution, and strong coupling at low energies [8, 9]. However, as pointed in Ref. [10], the dynamical behavior of the scalar is drastically improved when one consistently includes in the action all the possible operators that are allowed by the symmetry of the theory. There is only one of these operators at low energies, and its presence suffices to ensure dynamical consistency and to push strong coupling to sufficiently high energies, so that the theory makes sense as an effective theory. Strong coupling at high energies, which would still be a threat for UV completeness, persists in general [11, 12], but it appears to be avoided by assigning a specific hierarchy to the scales suppressing the lower and higher order operators [13]. There are many things to be worked out before HL gravity can be considered a viable UV complete gravity theory, such as renormalizability beyond power-counting, renormalization group flow of the various running couplings (so far infrared (IR) viability hinges on the hope that several parameters will run or can be tuned to desired values), various phenomenological aspects and constraints, etc. However, to date it certainly constitutes an interesting candidate.

Given that \mathfrak{a} -theory is a quite generic effective theory of LV gravity with a single preferred local timelike direction, it is reasonable to expect that the low energy limit of HL gravity will bear some resemblance to it. Indeed, it was remarked in Ref. [13] (see also Ref. [14]) and then fully demonstrated in Ref. [15] that, in the limit where higher than second order operators can be neglected, HL gravity is equivalent to \mathfrak{a} -theory with the extra condition that the aether is hypersurface orthogonal at the level of the action. Therefore, the IR limit of HL gravity can be understood as a limiting version of a well studied theory (some, though not all results carry over), which also gives hope that HL can be viable from the IR perspective. On the other hand, \mathfrak{a} -theory, or at least some version of it, acquires some more robust theoretical motivation as a low energy limit of a potentially UV complete gravity theory.

One of the results that carry over between the two theories is spherically symmetric solutions. This is because all spherically symmetric aether fields are hypersurface orthogonal and, hence, all spherically symmetric solutions of \mathfrak{a} -theory will also be solutions of the IR limit of HL gravity [15]. The converse holds for solutions with a regular center [16], but without this condition there may be additional HL solutions. Here we do not address that possibility, and instead focus entirely on black hole solutions to \mathfrak{a} -theory. Such solutions are interesting mathematically as black holes “dressed” by the aether. They can also be used in comparing these theories with observations of astrophysical black holes (though only as a first step since our solutions are non-rotating).

Motivated by this last point, our intention is to find, for each set of coupling parameters that meet current observational constraints, the unique static, spherically symmetric, vacuum, asymptotically flat black hole solution of \mathfrak{a} -theory that forms from collapse. Since different modes travel with different speeds in both \mathfrak{a} -theory and HL gravity, the definition of a “black hole” in these theories is potentially ambiguous. At the outset, our working definition will be that a black hole possesses both a metric horizon and a spin-0 mode horizon. We find, however, that in all of the several cases we have checked these solutions actually possess a “universal horizon,” not far inside the metric horizon, that traps modes of any speed.

We determine the black hole solutions numerically (using Mathematica), because obtaining analytic solutions of the equations does not appear to be feasible. As will be explained below, the restriction to black holes that form from collapse amounts to the requirement that the horizon for the superluminal spin-0 mode, which lies inside the metric horizon, is nonsingular. Our analysis generalizes the results of Ref. [17] which focused on a restricted, non-viable, choice of coupling parameters in the action, and the results of Ref. [18], which considered observationally viable coupling parameters, but did not impose regularity of the spin-0 horizon. Though other work has been done on black hole solutions in HL gravity, it was not in the same version of the theory considered here, but

in versions which either impose projectability (the lapse function is forced to be space-independent), *e.g.* Ref. [19], or consider only a reduced set of terms in the action, *e.g.* Refs. [20–22].¹ In contrast, as explained above, we include the complete set of terms in the IR limit. This changes the nature of the black hole solutions.

The rest of the paper is organized as follows. In section II we briefly review \mathfrak{a} -theory and HL gravity, as well as their relation. In section III we discuss the characteristics of generic spherically symmetric, asymptotically flat, black hole solutions and explain how the problem of generating numerical solutions can be set up. In section IV we summarize the various constraints we will take into account in order to restrict the parameter space in both \mathfrak{a} -theory and HL-gravity. We present and discuss numerical results in section V. Section VI contains our conclusions.

In this paper, we denote spacetime indices by Greek letters, and spatial indices by Latin letters. We also adopt the spacetime signature $(+---)$ and set $c = 1$.

II. \mathfrak{A} -THEORY AND HL GRAVITY: BRIEF OVERVIEW

The most general action for \mathfrak{a} -theory, up to total derivative terms and setting aside matter couplings, is

$$S_{\mathfrak{a}} = \frac{1}{16\pi G_{\mathfrak{a}}} \int \sqrt{-g} (-R + L_{\mathfrak{a}}) d^4x \quad (1)$$

where R is the 4D Ricci scalar of the metric g_{ab} , g is the determinant of the metric and

$$L_{\mathfrak{a}} = -M^{\alpha\beta}{}_{\mu\nu} \nabla_{\alpha} u^{\mu} \nabla_{\beta} u^{\nu}, \quad (2)$$

with $M^{\alpha\beta}{}_{\mu\nu}$ defined as

$$M^{\alpha\beta}{}_{\mu\nu} = c_1 g^{\alpha\beta} g_{\mu\nu} + c_2 \delta_{\mu}^{\alpha} \delta_{\nu}^{\beta} + c_3 \delta_{\nu}^{\alpha} \delta_{\mu}^{\beta} + c_4 u^{\alpha} u^{\beta} g_{\mu\nu}. \quad (3)$$

The c_i are dimensionless coupling constants, and it is assumed that u^{μ} is constrained to be a unit timelike vector, $g_{\mu\nu} u^{\mu} u^{\nu} = 1$. This constraint can be explicitly imposed with a Lagrange multiplier term $\lambda(g_{\mu\nu} u^{\mu} u^{\nu} - 1)$ in the action. Note that since the covariant derivative $\nabla_{\alpha} u^{\mu}$ involves derivatives of the metric through the connection components, and since the unit vector is nowhere vanishing, the terms quadratic in ∇u also modify the kinetic terms for the metric. One consequence of this is that the constant $G_{\mathfrak{a}}$ is related to Newton’s constant, as defined in the Newtonian limit, by [25]

$$G_N = \frac{G_{\mathfrak{a}}}{1 - (c_1 + c_4)/2}. \quad (4)$$

¹ The solutions found in Ref. [23] for HL gravity had been found earlier in Ref. [24] as solutions to \mathfrak{a} -theory and are not actually black hole solutions.

Varying the action (1) with respect to the metric yields

$$G_{\alpha\beta} = T_{\alpha\beta}^{\text{æ}} \quad (5)$$

where $G_{\alpha\beta} = R_{\alpha\beta} - Rg_{\alpha\beta}/2$ is the usual Einstein tensor. $T_{\alpha\beta}^{\text{æ}}$ denotes the aether stress-energy tensor

$$\begin{aligned} T_{\alpha\beta}^{\text{æ}} = & \nabla_{\mu} \left(J_{(\alpha}{}^{\mu} u_{\beta)} - J^{\mu}{}_{(\alpha} u_{\beta)} - J_{(\alpha\beta)} u^{\mu} \right) \\ & + c_1 [(\nabla_{\mu} u_{\alpha})(\nabla^{\mu} u_{\beta}) - (\nabla_{\alpha} u_{\mu})(\nabla_{\beta} u^{\mu})] \\ & + [u_{\nu}(\nabla_{\mu} J^{\mu\nu}) - c_4 \dot{u}^2] u_{\alpha} u_{\beta} \\ & + c_4 \dot{u}_{\alpha} \dot{u}_{\beta} - \frac{1}{2} L_{\text{æ}} g_{\alpha\beta}, \end{aligned} \quad (6)$$

where

$$J^{\alpha}{}_{\mu} = M^{\alpha\beta}{}_{\mu\nu} \nabla_{\beta} u^{\nu} \quad (7)$$

and $\dot{u}_{\nu} = u^{\mu} \nabla_{\mu} u_{\nu}$. Variation with respect to u^{μ} yields

$$(\nabla_{\alpha} J^{\alpha\nu} - c_4 \dot{u}_{\alpha} \nabla^{\nu} u^{\alpha})(g_{\mu\nu} - u_{\mu} u_{\nu}) = 0. \quad (8)$$

The Lagrange multiplier λ has been eliminated from these equations by solving for it using the aether field equation.

Suppose now we want to impose the restriction that the aether be hypersurface orthogonal. Locally, this amounts to saying that there exists a function T for which

$$u_{\alpha} = \frac{\partial_{\alpha} T}{\sqrt{g^{\mu\nu} \partial_{\mu} T \partial_{\nu} T}}, \quad (9)$$

where we have taken into account the unit constraint on the aether. If this form for the aether is substituted into the action (1), then one obtains a new theory, with fewer degrees of freedom, which is in fact identical to the IR limit of HL gravity. It appears from (2) and (9) that the resulting action would lead to equations of motion with fourth-order derivatives, and non-polynomial dependence on the derivatives. However, we can choose T itself to be the time coordinate t , in which case we have

$$u_{\alpha} = \delta_{\alpha}^T (g^{TT})^{-1/2} = N \delta_{\alpha}^T, \quad (10)$$

where $N = (g^{TT})^{-1/2}$ is the lapse function. Moreover, the equation of motion that would come from variation of T is identically satisfied when the metric and matter equations of motion are imposed, hence this gauge choice can be made before varying T (see Ref. [15] for more details).

This hypersurface-orthogonal æ-theory action then takes the form

$$S_{h.o.\text{æ}} = \frac{1}{16\pi G_H} \int dT d^3x N \sqrt{h} L_2 \quad (11)$$

with

$$L_2 = K_{ij} K^{ij} - \lambda K^2 + \xi^{(3)} R + \eta a_i a^i, \quad (12)$$

where K^{ij} is the extrinsic curvature of each constant T surface, h_{ij} is the induced spatial metric, ${}^{(3)}R$ its Ricci curvature, and

$$a_i = \partial_i \ln N \quad (13)$$

is the spatial projection of the acceleration of the normal congruence, *i.e.* the acceleration of the aether flow. The correspondence of the various parameters is²

$$\frac{G_H}{G_{\text{æ}}} = \xi = \frac{1}{1 - c_{13}}, \quad \lambda = \frac{1 + c_2}{1 - c_{13}}, \quad \eta = \frac{c_{14}}{1 - c_{13}}, \quad (14)$$

where we use the notation $c_{ij} = c_i + c_j$.

Note that the coupling constants c_1 , c_3 and c_4 enter only through the combinations c_{13} and c_{14} . This can be traced to a redundancy in the terms of the action when the aether is hypersurface orthogonal. This is relevant both for HL gravity, and for æ-theory in spherical symmetry, since any spherically symmetric vector field is hypersurface orthogonal. The twist $\omega_{\alpha} = \epsilon_{\alpha\beta\gamma\delta} u^{\beta} \nabla^{\gamma} u^{\delta}$ vanishes for any such vector field. For a unit vector field, the square of the twist is given by

$$\begin{aligned} \omega_{\alpha} \omega^{\alpha} = & -(\nabla_{\alpha} u_{\beta})(\nabla^{\alpha} u^{\beta}) + (\nabla_{\alpha} u_{\beta})(\nabla^{\beta} u^{\alpha}) \\ & + (u^{\beta} \nabla_{\beta} u_{\alpha})(u^{\mu} \nabla_{\mu} u^{\alpha}). \end{aligned} \quad (15)$$

As far as solutions with zero twist are concerned, any multiple of $\omega_{\alpha} \omega^{\alpha}$ can be added to the action (1) without changing the solutions. For example, adding $c_1 \omega_{\alpha} \omega^{\alpha}$ results in new couplings $c'_1 = 0$, $c'_3 = c_{13}$, and $c'_4 = c_{14}$. This shows that the hypersurface orthogonal solutions depend only on c_2 , c_{13} , and c_{14} . Alternatively, one can subtract $c_4 \omega_{\alpha} \omega^{\alpha}$ from the action, eliminating the c_4 term. We will do this in the calculations that follow.

Having fixed the T coordinate up to a global reparametrization (under which u_{α} (9) is invariant), the symmetry of the theory is reduced to that of ‘‘foliation preserving diffeomorphisms,’’ *i.e.* space-independent time reparametrization together with time-dependent spatial diffeomorphisms,

$$T \rightarrow T'(T), \quad x^i \rightarrow x'^i(x^i, T). \quad (16)$$

Under these transformations $N' dT' = N dT$, and $a'_i = a_i$. The action (11) is the most general one that is invariant under these symmetries and involves no more than two derivatives of N and g_{ij} .

As already mentioned, the above theory is the IR limit of HL gravity. The full HL action is of the form

$$S_{HL} = \frac{1}{16\pi G_H} \int dT d^3x N \sqrt{h} \left(L_2 + \frac{1}{M_{\star}^2} L_4 + \frac{1}{M_{\star}^4} L_6 \right), \quad (17)$$

² A rescaling of the spatial metric can be used to set $\xi = 1$ in the absence of matter, as sometimes done in the literature. This is no longer possible once matter is present.

where M_* is a new mass scale, and L_4 and L_6 include all the foliation preserving diffeomorphism invariant scalar functions of a_i and h_{ij} of 4th and 6th order in the spatial derivatives, respectively. The presence of 6th order operators is crucial for power counting renormalizability [7]. On the other hand, in the absence of extra symmetries, radiative corrections will generate all possible terms up to this order [9, 10]. In particular, the term $a_i a^i$ in L_2 is crucial for the improved dynamical behavior of the theory [10].

It has been argued that if the mass M_* lies somewhere between roughly 10^{10}GeV and 10^{16}GeV the theory can both avoid strong coupling, and satisfy gravitational constraints and generic LV constraints in the matter sector [16] (the need to alleviate strong coupling imposes the upper bound [11, 13] which is competing with the lower bounds coming from LV violations, as first pointed out in Ref. [11]). Thus, at low energy one expects to be able to neglect the higher order operators in L_4 and L_6 , so in this sense the action (11) is the low energy limit of the action (17). We can thus say that the low energy or IR limit of HL gravity is equivalent to \mathcal{A} -theory with a hypersurface orthogonal aether.

It is worth mentioning that, since L_4 and L_6 contain higher spatial derivatives of the fields, a theory described by action (17) can have solutions that are perturbatively far from solutions of the theory described by action (11) and which diverge as M_* goes to infinity, if the derivatives of the fields are large enough. That is, theory (17) can have more solutions than theory (11) when contributions coming from L_4 and L_6 are important.

III. STATIC, SPHERICALLY SYMMETRIC, ASYMPTOTICALLY FLAT, REGULAR BLACK HOLES

A. Horizons and field redefinition

In this section we briefly review the field and coupling constant redefinitions that we perform in order to simplify our calculations. Such redefinitions closely follow those used in Ref. [17], to which we refer for a more detailed discussion.

\mathcal{A} -theory possesses spin-2, spin-1 and spin-0 propagating degrees of freedom, whereas HL gravity has only spin-2 and spin-0 modes. However, once spherical symmetry has been imposed, only the spin-0 mode is relevant. The squared speed (at low energies for HL gravity) of this mode, defined relative to the aether rest frame, is [26]

$$s_0^2 = \frac{c_{123}(2 - c_{14})}{c_{14}(1 - c_{13})(2 + c_{13} + 3c_2)}. \quad (18)$$

Since different modes propagate at different speeds there will be multiple (causal) horizons. In fact for each of these modes the corresponding horizon will be a null surface of the effective metric

$$g_{\alpha\beta}^{(i)} = g_{\alpha\beta} + (s_i^2 - 1)u_\alpha u_\beta, \quad (19)$$

where s_i is the speed of the spin- i mode. See Ref. [17] for a more detailed discussion.

The action (1) is invariant under the combined metric and aether field redefinition

$$g'_{\alpha\beta} = g_{\alpha\beta} + (\sigma - 1)u_\alpha u_\beta, \quad (20)$$

$$u'^\alpha = \frac{1}{\sqrt{\sigma}}u^\alpha, \quad (21)$$

provided that the c_i are replaced by new parameters \tilde{c}_i which are functions of the initial c_i (see Ref. [27] for the exact correspondence). By choosing $\sigma = s_0^2$ we can make the spin-0 horizon coincide with the metric horizon of the redefined metric. This will help to simplify the calculations.

As explained in the previous section, when spherical symmetry is imposed the aether is hypersurface orthogonal, and so it has vanishing twist. Thus by making use of Eq. (15) it is possible to set c_4 to zero without loss of generality. It is worth stressing that this procedure has to come after the field redefinition described previously to make the spin-0 horizon coincide with the metric horizon. If the order were to be reversed, the field redefinition would regenerate a c_4 term.

B. Asymptotics, regularity and parameters of solutions

We find it convenient to work in Eddington-Finkelstein-like coordinates with the line element

$$ds^2 = F(r)dv^2 - 2B(r)dvdr - r^2 d\Omega^2, \quad (22)$$

as these coordinates are regular at both the metric and the spin-0 horizon, as well as in the interior region of the black hole. We stress that from Eq. (22) it follows that the radial coordinate has a geometric meaning, namely $4\pi r^2$ is the area of a symmetry sphere. The aether field can be written in the form

$$u^\alpha \partial_\alpha = A(r)\partial_v - \frac{1 - F(r)A^2(r)}{2B(r)A(r)}\partial_r, \quad (23)$$

where we have imposed the unit constraint. For static, spherically symmetric solutions these ansätze for the metric and the aether can be adopted without loss of generality. Surfaces of constant v are null, and if we think of v as increasing in the future direction at fixed r , it is an ingoing null coordinate. The timelike vector u is then future pointing provided $A > 0$. The Lagrangian (2) is even in u , hence in any solution we can also replace u by $-u$, which amounts to replacing A by $-A$. Thus, a black hole with aether flowing in can also be viewed as a white hole with aether flowing out.

In GR, according to Birkhoff's theorem, there is a one parameter family of spherically symmetric solutions, namely the Schwarzschild solutions, labeled by the mass. These solutions are asymptotically flat, and static. In

\mathfrak{a} -theory there is a scalar mode, corresponding to radial tilting of the aether, so that Birkhoff's theorem does not apply. Not only are spherical solutions not generally static, but even if we restrict to static, spherical solutions, they are not necessarily asymptotically flat. In fact, as shown in Ref. [17], there is a three parameter family of such solutions, and imposing asymptotic flatness reduces this to a two parameter family. That is, for each mass, there is a one parameter family. As explained below, we will fix this parameter by the condition that the spin-0 horizon, *i.e.* the outermost trapped surface for spin-0 waves, be nonsingular.

A series expansion for the static, spherically symmetric, asymptotically flat solutions was previously found for the case $c_3 = -c_1$ [17], and we have found that this series remains valid with no restriction on c_3 . The result, given in terms of the inverse radial coordinate $x = 1/r$, is

$$F(x) = 1 + F_1 x + \frac{1}{48} c_{14} F_1^3 x^3 + \dots \quad (24)$$

$$B(x) = 1 + \frac{1}{16} c_{14} F_1^2 x^2 - \frac{1}{12} c_{14} F_1^3 x^3 + \dots \quad (25)$$

$$A(x) = 1 - \frac{1}{2} F_1 x + A_2 x^2 + \left(-\frac{1}{96} c_{14} F_1^3 + \frac{1}{16} F_1^3 - F_1 A_2 \right) x^3 + \dots \quad (26)$$

where $F_1 = F'(x=0)$ and $A_2 = A''(x=0)$, and where v is scaled to set $F(x=0) = 1$. No more free parameters seem to appear at higher orders, so the asymptotically flat solutions are determined by the two free parameters F_1 and A_2 . The parameters c_2 and c_3 enter at higher orders in $1/r$. Their absence at lower orders is presumably related to the fact that they do not appear *at all* in solutions whose aether is everywhere aligned with the timelike Killing vector [24].

We will restrict attention in this paper to the values of the coupling coefficients c_i in the action for which presently known observational bounds are all met. Even though section IV is devoted to a discussion about these bounds and the restrictions they will bring to the parameter space, we anticipate here the discussion of a particular constraint: the vacuum Čerenkov constraint [28], which amounts to the requirement that the speed of the spin-0 mode be greater than or equal to the speed of light ($c = 1$) defined by the metric cone. This means that the spin-0 horizon lies inside the metric horizon. If matter is minimally coupled to the metric then the matter cannot propagate beyond the metric cone, and the spin-0 horizon is hidden from view, except by gravitational and aether signals. Nevertheless, we shall require that the spin-0 horizon be regular, simply because the evidence we have indicates that when a black hole forms in a collapse process, the spin-0 horizon is in fact nonsingular. This evidence amounts to the argument that nothing singular is happening in the fields at that point, bolstered by numerical simulations for a few examples [29], although a general proof has not been given. If instead collapse does *not* automatically impose this condition, a black

hole would have “hair” determined by the parameter A_2 in Eq. (26).

Having imposed asymptotic flatness, and a regular spin-0 horizon, there remains a one parameter family of solutions, *i.e.* one solution for each value of the total mass. Equivalently, the solutions can be parametrized by the horizon radius. If we adopt units for the radial coordinate in which the horizon radius is unity, this leaves a unique solution. This is the solution we are characterizing in the present paper, as a function of the couplings c_i .

C. Equations and constraints

In this section we discuss the set of equations to be integrated. The equations to be solved are the generalized Einstein equations (5), for which we introduce the notation

$$E^{\mu\nu} \equiv G^{\mu\nu} - T_{\mathfrak{a}}^{\mu\nu} = 0, \quad (27)$$

and the aether field equations (8), for which we introduce the notation

$$\mathfrak{A}^\mu = 0. \quad (28)$$

Given the spherical symmetry and staticity, many of these equations are redundant or trivial, and it suffices to impose

$$E^{vv} = E^{vr} = E^{rr} = E^{\theta\theta} = \mathfrak{A}^v = 0, \quad (29)$$

each of which must hold at every value of r . (In particular, \mathfrak{A}^r is proportional to \mathfrak{A}^v so need not be separately imposed.) All these equations involve second derivatives of F and A (but not B) with respect to r . However, note that there are only three functions to be solved for, F , B , and A , so only three equations are needed to determine a solution, given initial data. In fact, among these five equations, two independent combinations are initial value constraint equations, relating the functions and their first derivatives. The constraint equations automatically hold at all values of r , if they are imposed at one value of r , as a consequence of the remaining “evolution” equations.

To clarify the distinction between constraints and evolution equations in both \mathfrak{a} -theory and HL gravity, it is useful to recall how that distinction comes about in GR in the general case (*i.e.*, in the absence of symmetries). In the absence of matter, the field equations of GR are given by the vanishing of the Einstein tensor, $G^{\mu\nu} = 0$. Because of diffeomorphism invariance, there are four free functions in the time evolution of the metric, which is therefore not uniquely determined from initial data. This means that not all of the Einstein equations can be evolution equations. Indeed, the Einstein tensor satisfies the contracted Bianchi identity

$$\nabla_\mu G^{\mu\nu} = 0, \quad (30)$$

which holds independently of any field equations and can also be seen as a consequence of the diffeomorphism invariance of the Einstein–Hilbert action. Expanding this equation in components in a coordinate system (t, x^i) one has

$$\partial_t G^{t\nu} + \partial_i G^{i\nu} + \Gamma G\text{-terms} = 0. \quad (31)$$

This identity implies that if $G^{\mu\nu} = 0$ at some initial “time” t_0 , then $G^{t\nu} = 0$ also holds at $t = t_0 + \delta t$. Thus if the equations $G^{t\nu} = 0$ are imposed at some initial time t_0 , they are satisfied in the whole spacetime when the remaining equations hold. Moreover, the quantities $G^{t\nu}$ involve only initial values. This follows from the fact that if a given field component appears in $G^{\mu\nu}$ with up to n time derivatives, then Eq. (31) – being an identity that holds for all metrics independent of field equations – implies that $G^{t\nu}$ has no more than $n - 1$ time derivatives of that field component. Thus the equations $G^{t\nu} = 0$ are *initial value constraint equations*.

The discussion of initial value constraint equations can be extended to cover the case when matter is coupled to the metric. We will discuss that extension explicitly here just for the case when the “matter” corresponds to the aether degrees of freedom in \mathfrak{a} -theory. The corresponding Einstein equation (27) involves second time derivatives of the aether field u^μ in $T_{\mathfrak{a}}^{\mu\nu}$ [see Eq (6)]. These arise from the variation of the metric in the Christoffel symbols occurring in the covariant derivatives of the aether field. The equations $E^{t\nu} = 0$ are therefore clearly not initial value equations, even though the on-shell identity $\nabla_\mu E^{\mu\nu} = 0$ implies that if they hold initially they continue to hold as a result of the remaining equations.³ Instead, to identify true initial value constraint equations we need to find a true identity, analogous to the Bianchi identity, that holds independent of any field equations.

Such an identity can be found by using the diffeomorphism invariance of the full \mathfrak{a} -theory action.⁴ One finds

$$\nabla_\mu (E^{\mu\nu} - u^\mu \mathfrak{A}^\nu) = \mathfrak{A}_\mu \nabla^\nu u^\mu, \quad (32)$$

where the normalization of the aether field equation is defined by $\delta S/\delta u^\mu = 2\mathfrak{A}_\mu$. This identity can be used to argue, in a way identical to that used for vacuum GR, that

$$E^{t\nu} - u^t \mathfrak{A}^\nu = 0 \quad (33)$$

are initial value constraint equations.

The reasoning presented above applies as well to the static, spherically symmetric case, with the role of t -evolution replaced by r -evolution. Hence we now define

the constraint equations as

$$C^\nu \equiv E^{r\nu} - u^r \mathfrak{A}^\nu = 0. \quad (34)$$

It follows from the reasoning just given that, once imposed at a single initial radius, these equations are automatically satisfied at all r provided that the remaining field equations hold. Also, they depend only on initial data (with respect to r -evolution). To exploit this structure, we therefore replace the set of equations (29) by the equivalent set

$$E^{v\nu} = E^{\theta\theta} = \mathfrak{A}^v = 0, \quad C^v = C^r = 0. \quad (35)$$

The first three equations can be recast in the form

$$F'' = F''(A, A', B, F, F') \quad (36)$$

$$A'' = A''(A, A', F, F') \quad (37)$$

$$B' = B'(A, A', B, F, F'), \quad (38)$$

which is a system of ordinary differential equations (ODEs) that can be numerically integrated with respect to r . These equations will be our “evolution” equations. The constraint equations $C^v = C^r = 0$, instead, depend only on A, A', B, F and F' . Therefore they simply impose algebraic constraints on the data at the “initial” radius r_0 , and are automatically preserved by the evolution equations for any other r .

D. Numerical implementation

As explained in section III B, imposing asymptotic flatness, together with the condition that there is a regular spin-0 horizon, will lead to a one parameter family of solutions. These describe black holes, because for the theory parameters that we consider there will be a metric horizon outside the spin-0 horizon. We begin the integration at the location of the spin-0 horizon, where the regularity condition can be imposed directly on the initial data, as was done in Ref. [17]. To conveniently implement this procedure, as in Ref. [17], we first make a field redefinition so that the spin-0 metric, Eq. (19) with $s_i = s_0$, is the new metric. (This induces a change in the coupling parameters, which we keep track of.) Then the spin-0 horizon coincides with the metric horizon at $r = r_H$, which is defined by the condition

$$F(r_H) = 0. \quad (39)$$

We adopt units in which $r_H = 1$, so the one-parameter family is represented with just a single solution to be found. After finding the solution, we then make the inverse of the field redefinition (20) to express the solution in terms of the original metric that is assumed to be minimally coupled to the matter fields, and the corresponding aether field.

To impose regularity of the horizon we proceed as follows. The evolution equation for B' [Eq. (38)] turns out to have the structure

$$B' = b_0/F + b_1 + b_2 F, \quad (40)$$

³ Note that $G^{t\nu} - 8\pi T^{t\nu} = 0$ are indeed initial value constraint equations in settings where the matter stress tensor $T^{\mu\nu}$ has fewer derivatives than the matter equations of motion.

⁴ The precise origin of this identity, and its generalization to other theories with tensor matter, will be explained in a forthcoming publication.

where $b_{0,1,2}$ are functions of (A, A', B, F') . Therefore, B' diverges at r_H unless

$$b_0(A, A', B, F')|_H = 0. \quad (41)$$

(Here and below, we shall denote quantities evaluated at r_H using the subscript H , *e.g.* $F_H \equiv F(r_H)$.) Once the constraint in Eq. (41) is imposed, both the metric and aether are regular at the horizon.

The system of evolution equations (36)–(38) requires a five dimensional space of initial conditions, $(A, A', B, F, F')_H$, but we also have to impose the constraint equations $C^r = C^v = 0$. Once we impose the horizon and regularity conditions Eqs. (39) and (41), the constraint equation $C^r = 0$ is automatically satisfied at r_H , as it is proportional to F . The other constraint equation $C^v = 0$, however, is not trivially satisfied at r_H , and further restricts the initial conditions:

$$C^v(A, A', B, F')|_H = 0. \quad (42)$$

Together with the other conditions in Eqs. (39) and (41), this cuts the space of initial conditions from five down to two dimensions. This is further reduced to one dimension by choosing to scale the coordinate v so as to have $B_H = 1$. We can then parametrize the space of initial data with the value of A on the horizon, A_H .

A generic value of A_H will not lead to an asymptotically flat solution. As in Ref. [17], we seek the value of A_H leading to asymptotic flatness using a “shooting method”. In practice, we integrate out from r_H starting with different values of A_H , until we find both a value of A_H that gives $FA^2 > 1$ far away from the horizon, and one which instead gives $FA^2 < 1$. This is sufficient to “bracket” the asymptotically flat solution, which as can be seen from Eqs. (24)–(26) satisfies $\lim_{r \rightarrow \infty} FA^2 = 1$. (Note that the quantity FA^2 is invariant under rescalings of r and v , which justifies its use in our code, where we choose specific scalings for these coordinates). Once the two bracketing values of A_H have been identified, a simple bisection procedure will yield the asymptotically flat black hole with higher and higher accuracy.

In principle this completes the description of our integration procedure. However there are some complications that affect how it is actually implemented in our code. We now describe these complications and the implementation.

First, the value of A_H does not uniquely fix all the initial conditions through Eqs. (39), (41) and (42), since the latter two are quadratic in F'_H and A'_H . These can be linearly combined to obtain a linear equation for F'_H , but when replacing the solution into Eq. (41) or (42) one obtains a quartic equation in A'_H . Thus one A_H determines four values for A'_H (and F'_H , which depends on A'_H).

Since F must asymptote to a positive value at spatial infinity to achieve asymptotic flatness, we can readily discard the branches that give $F'_H < 0$, otherwise F would then have another zero (*i.e.*, another horizon, possibly

singular) outside r_H . However, this still does not select a unique branch, and we are typically left with at least two branches that can potentially give an asymptotically flat black hole with no horizons outside r_H . We find, however, that for any given set of the theory’s parameters, only one branch seems to give rise to an asymptotically flat black hole, the other branches failing to give a viable bracketing interval for A_H . Because the branch that gives the asymptotically flat solution is typically not the same (as labeled by Mathematica) as the parameters of the theory are varied, in practice we proceed in the following manner. We start off with a theory parametrically close to GR, where we can easily identify the branch that evolves to an asymptotically flat solution, that being the branch that gives a value of F'_H close to the GR value $F'_H = 1/r_H = 1$. [The other branches give instead very large values for F'_H , and they fail at providing a bracketing interval for $A(r_H)$.] We then gradually move away from GR, varying the coupling parameters c_i by a small amount, and identifying the branch that is closest to the one that worked for the previous values of c_i . While this procedure might in principle miss the existence of another branch of asymptotically flat black hole solutions, that seems unlikely in view of the tests that we conducted on the remaining branches, none of which seems to produce such solutions.

Another difficulty stems from the regularity condition (41). While this equation ensures that B' is non-singular on the horizon, Eq. (40) can potentially be affected by numerical inaccuracies when evaluated very close to the horizon. This is because both b_0 and F are zero on the horizon, but are non-zero (albeit small) at radii r very close to r_H . As a result, B' will not be calculated accurately at such radii, due to the finite machine accuracy of any calculator. While it might be possible to overcome this problem by cranking up the number of significant digits used by the code, a more elegant and robust approach is to integrate the evolution equations perturbatively near the horizon, *i.e.* to expand them in a series in $r - r_H$ and solve them analytically order by order, as in Ref. [17]. We did so up to seventh order in $r - r_H$ using Mathematica, and used this perturbative solution from $r_H = 1$ to $r_{\text{in}} = 1.001$. The error of the perturbative solution at $r_{\text{in}} = 1.001$ is therefore $\mathcal{O}(r_{\text{in}} - r_H)^8 \sim 10^{-24}$, comparable to the machine accuracy (we use 22 significant digits for our real numbers, which is possible using Mathematica). We can then integrate the evolution equations numerically from r_{in} up to very large radii ($r \sim 10^4$ or larger) using Mathematica’s default ODE integrator (which automatically switches between backward differentiation formulas and Adams multistep methods depending on the equations’ stiffness). Because the evolution equations (36)–(38) are lengthy and complicated, we evaluate their right-hand sides with 22 significant digits in order to minimize the impact of round-off errors, and we set the accuracy and the precision goal of the ODE integrator to 10^{-15} . As a confirmation that the integration is performed accurately,

we check that the constraints C^v and C^r are preserved to within 10^{-12} or better. More specifically, the dimensionless quantities $|C^v r^2|$ and $|C^r r^2|$ remain smaller than 10^{-12} during the whole evolution.

Using this set-up, we can then finely bracket the asymptotically flat solution. (We stop our bisection either when the value $A(r_H)$ giving an asymptotically flat solution is determined to within 10^{-22} or when the two bracketing solutions agree to within 10^{-15} .) As final confirmation of the accuracy of our procedure, we rescale the time v so that F approaches 1 asymptotically, and then verify that our solution agrees well with the asymptotic solution (24)–(26).

IV. PARAMETER SPACE

Even after the parameter redefinition to eliminate c_4 in \mathfrak{a} -theory described in section II, one is left with a 3-dimensional parameter space. Similarly, in HL gravity one has to deal with a 3-dimensional parameter space *a priori*. Scanning such a space is clearly a formidable task. Fortunately, there are certain regions of the parameter space which are far more interesting than others, as there are a number of viability constraints that one can impose on both theories, namely:

1. *Classical and quantum-mechanical stability*: all propagating modes should be classically stable and have positive energy (no tachyons, no ghosts).
2. *Avoidance of vacuum Čerenkov radiation by matter* [28]: this requires that the squared speeds of the propagating modes should be greater than or equal to unity.
3. *Agreement with GR at first post-Newtonian order*: (This implies, in particular, that all the constraints coming from Solar system experiments are met.) The parametrized post-Newtonian (PPN) parameters of both \mathfrak{a} -theory and low-energy HL gravity are identical to those of GR with the exception of those measuring preferred frame effects, α_1 and α_2 [16, 30]. These two parameters are constrained to be below 10^{-4} and 10^{-7} respectively [31].

Note that constraints 2 and 3 refer implicitly to the metric to which matter couples minimally. Hence we must impose these constraints on the coupling parameters *before* making the field redefinition (20). In what comes next we explore only the part of the parameter space that satisfies all of the above constraints. Additionally, we impose a stronger version of 3, namely $\alpha_1 = \alpha_2 = 0$, so that the two theories are indistinguishable from GR at the first order PPN level. (This requirement is reasonable given that the bounds on α_1 and α_2 are very strong, as mentioned above.)

The bound imposed on the c_i by the above constraints have been summarized in Ref. [5] for \mathfrak{a} -theory. The con-

dition $\alpha_1 = \alpha_2 = 0$ translates to

$$c_2 = \frac{-2c_1^2 - c_1 c_3 + c_3^2}{3c_1}, \quad (43)$$

$$c_4 = -\frac{c_3^2}{c_1}, \quad (44)$$

which reduces the parameter space down to 2 dimensions. In terms of $c_{\pm} = c_1 \pm c_3$, then constraints 1 and 2 are satisfied in the region

$$0 \leq c_+ \leq 1, \quad (45)$$

$$0 \leq c_- \leq \frac{c_+}{3(1-c_+)}. \quad (46)$$

For practical purposes, and given that larger values are unlikely to be compatible with strong field constraints from binary pulsar systems [32], we will explore the part of this region which also satisfies $c_- \leq 1$.

An important observational constraint that has not been included in the list above is that related to gravitational radiation from binary pulsars. As shown in Refs. [32, 33], when the preferred frame PPN parameters α_1 and α_2 vanish, as assumed here, and when gravitational fields are everywhere weak or the coupling constants c_i are smaller than something of order $\sim 0.01-0.1$, all gravitational radiation is sourced by the quadrupole Q_{ij} , as in GR. The net power radiated in all modes is then given by $(G_N \mathcal{A}(c_i)/5) \ddot{Q}_{ij}^2$. Agreement with the damping rate of GR requires $\mathcal{A}(c_i) = 1$, which would impose an extra relation between the c_i . Even though we have not used this constraint to further restrict the parameter space, we present the curve $\mathcal{A}(c_i) = 1$ in some of the figures that follow, but only for $c_+ < 0.1$, as for larger values the damping rate for compact binaries is not accurately given by this formula [32].

We now move to HL gravity. The PPN constraints were worked out in Ref. [16], but a different parametrization (μ, α, β) of the action was used (what we denote here as μ was actually denoted by λ' in Ref. [16]). The relation with the more common parametrization used in Eq. (11) is given by

$$\xi = \frac{1}{1-\beta}, \quad \lambda = \frac{1+\mu}{1-\beta}, \quad \eta = \frac{\alpha}{1-\beta}. \quad (47)$$

The relation with the \mathfrak{a} -theory parameters, given by (14), is

$$\alpha = c_{14}, \quad \beta = c_{13}, \quad \mu = c_2. \quad (48)$$

The condition $\alpha_1 = \alpha_2 = 0$ is satisfied when $\alpha = 2\beta$, and again the parameter space becomes 2-dimensional. Then constraints 1 and 2 above are satisfied in the following 3 regions of the (μ, β) plane

$$0 < \beta < 1/3, \quad \mu > \frac{\beta(\beta+1)}{1-3\beta}, \quad (49)$$

$$0 < \beta < 1/3, \quad \mu < -\frac{2+\beta}{3}, \quad (50)$$

$$1/3 < \beta < 1, \quad \frac{\beta(\beta+1)}{1-3\beta} < \mu < -\frac{2+\beta}{3}. \quad (51)$$

(Note that the two last regions are actually connected, forming one single region.) We will explore all of these regions but for practical purposes we will restrict to $|\mu| < 10$.

In terms of the (ξ, λ, η) set of parameters, the PPN condition $\alpha = 2\beta$ becomes $\eta = 2(\xi - 1)$, and Eqs. (49)–(51) translate to

$$\frac{3\lambda - 1}{2\lambda} > \xi > 1, \quad \lambda > 1 \quad \text{or} \quad \lambda < 0, \quad (52)$$

$$\xi > 1, \quad 0 < \lambda < 1/3. \quad (53)$$

V. NUMERICAL SOLUTIONS

A. Comparison to known black-hole solutions in \mathfrak{a} -theory

As a first test of our code, we tried to reproduce the \mathfrak{a} -theory regular black-hole solutions studied in Ref. [17]. In that paper, Eling & Jacobson focused on \mathfrak{a} -theories with $c_3 = c_4 = 0$ in order to simplify the (very complicated) field equations. Additionally, they imposed the condition $c_2 = -c_1^3/(3c_1^2 - 4c_1 + 2)$, which ensures that $s_0 = 1$, so that the metric horizon coincides with the spin-0 horizon. After these simplifying assumptions the preferred frame PPN parameter α_1 vanishes. However, the observational bound on the second preferred frame parameter, $\alpha_2 < O(10^{-7})$, leads to the constraint $|c_1|, |c_2| < O(10^{-7})$. The values for c_1 considered in Ref. [17] were actually significantly larger, making the theories considered there non-viable. (Even if one identifies the theories studied in Ref. [17] with the “redefined”

Table I: Properties of regular black hole solutions with $c_3 = c_4 = 0$ and c_2 such that $s_0 = 1$. GR corresponds to $c_1 = 0$. See text for explanation of the quantities shown.

c_1	r_g/r_H	$F'_H A_H^2$	$\gamma_{\#}$
0	1	n/a	n/a
0.1	0.989489	2.09612	1.60280
0.2	0.978021	2.07168	1.57695
0.3	0.965229	2.03920	1.54768
0.4	0.950547	1.99652	1.51409
0.5	0.933044	1.94056	1.47484
0.6	0.911068	1.86668	1.42796
0.7	0.881313	1.76732	1.37024
0.8	0.835830	1.62834	1.29591
0.9	0.747519	1.41557	1.19212
0.91	0.733012	1.38702	1.17904
0.92	0.716505	1.35637	1.16523
0.93	0.697454	1.32324	1.15060
0.94	0.675075	1.28711	1.13502
0.95	0.648165	1.24724	1.11831
0.96	0.614764	1.20248	1.10023
0.97	0.571331	1.15094	1.08044
0.98	0.510382	1.08891	1.05834
0.99	0.410630	1.00689	1.03281

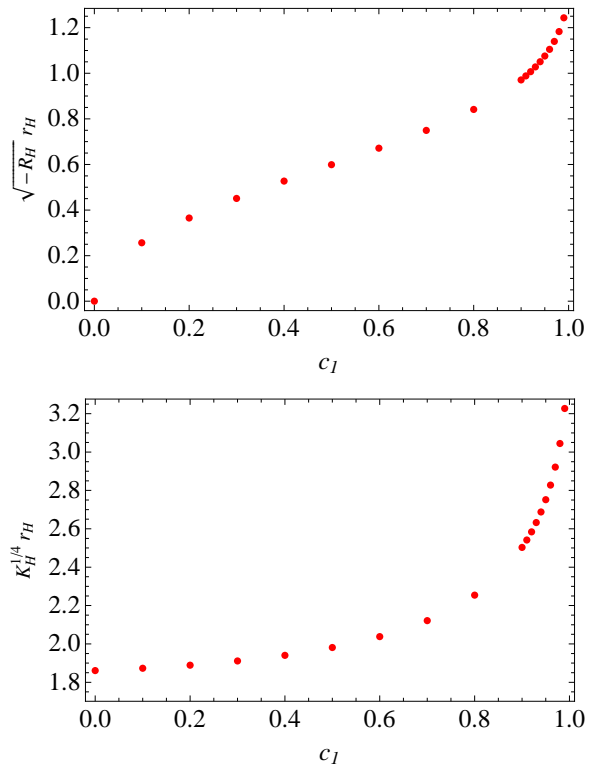


Figure 1: The curvature radius on the horizon, in units of the horizon’s circumference radius r_H . More specifically, R_H and K_H denote the Ricci and Kretschmann scalars evaluated on the horizon.

theory of Sec. III A, they do not lead to viable theories in the “physical” parameter space. One should mention, however, that the purpose of Ref. [17] was to understand the properties of regular \mathfrak{a} -theory black holes in a simple family of “test-theories”, even at the cost of sacrificing their viability.)

Ref. [17] focused on theories with $c_1 > 0$ (since $c_1 < 0$ would give negative spin-0 mode energy), but found no regular solutions for $c_1 > 0.7$. Our code, instead, finds regular black-hole solutions in the whole range $0 < c_1 < 1$. While it is not clear why the solutions for $0.7 < c_1 < 1$ were not found by the code of Ref. [17] — nor why they were not produced in the gravitational-collapse simulations of Ref. [29], which confirmed that no regular BHs seemed to form in theories with $c_1 > 0.8$ — our code produces, even in this region of the parameter space, regular BHs that are very accurate solutions of the field equations and that agree with the asymptotically flat analytical solution (24)–(26) (see Sec. III D).

One possibility is that the code of Ref. [17] was simply not accurate enough: because of the lengthy field equations, rounding errors can propagate and lead to significant inaccuracies if one does not use a sufficient number of significant digits. (For this work, as stressed in Sec. III D, we use real numbers with 22 significant dig-

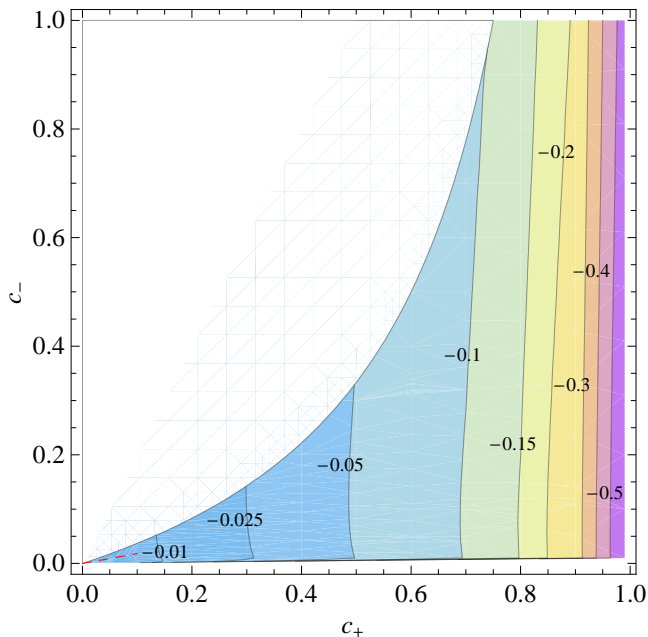


Figure 2: Fractional æ-theory deviation from GR for the dimensionless product $\omega_{\text{ISCO}} r_g$ of the ISCO frequency and the gravitational radius, in the viable region of the parameter plane (see Sec. IV). The red dashed line extending up to $c_+ \approx 0.1$ is the binary pulsar constraint $c_- \approx 0.18c_+$.

its). To gauge the accuracy of the code of Ref. [17], we compare the numerical solutions found there with those that we find with our code. In particular we look at three quantities that were used in Ref. [17] to characterize the solutions, namely (i) the ratio r_g/r_H (which equals 1 in GR), where r_H is defined geometrically as the proper circumference of the horizon divided by 2π , and where r_g is the “gravitational radius,” *i.e.* the parameter that appears in the asymptotic form of the metric, $F = 1 - r_g/r + O(1/r^2)$; in terms of the mass M_{tot} as measured by a distant observer we have

$$r_g = 2G_N M_{\text{tot}}; \quad (54)$$

(ii) the combination $F'_H A_H^2$, which is invariant under a rescaling of the coordinate time $v \rightarrow \chi v$; (iii) the Lorentz factor $\gamma_{\text{ff}} = u^\mu u_\mu^{\text{obs}}$ of the æther, defined with respect to a unit Killing energy radial observer at the horizon (u_μ^{obs} is tangent to a radial free-fall trajectory that starts at rest at spatial infinity).

These quantities are reported in Table I as function of c_1 (GR corresponds to $c_1 = 0$), for the solutions that we find in the range $0 < c_1 < 1$. A comparison with Table I of Ref. [17] shows that the values of r_g/r_H only agree up to the third decimal digit for $c_1 \leq 0.3$. This difference is much larger than our estimated error on r_g/r_H , which is less than 2 parts in 10^{14} and which we obtain from the bracketing procedure described in Sec. IIID. This suggests that our code might be more accurate than that of Ref. [17], which could explain why we find solutions

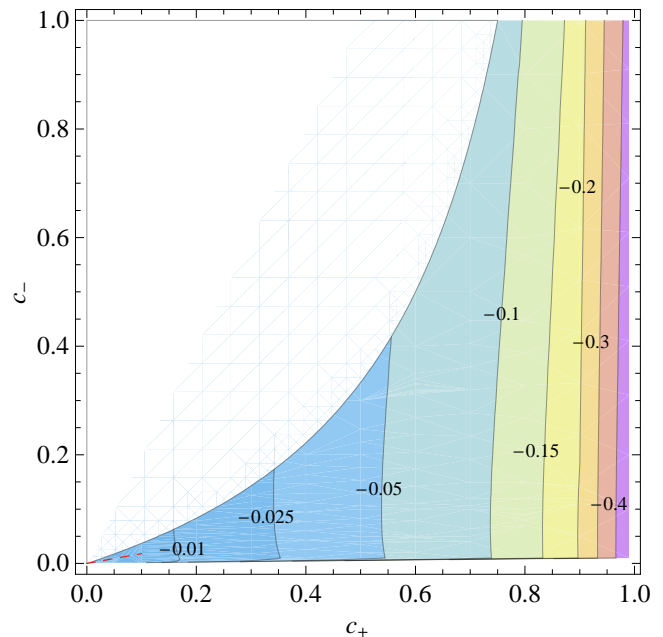


Figure 3: Same as Fig. 2, but for the maximum redshift of a photon emitted by a source moving on the ISCO, $z_{\text{max}} = \nu_{\text{emitted}}/\nu_{\text{measured}} - 1$. This maximum redshift is obtained for a photon emitted “backward” with respect to the velocity of the source.

up to $c_1 = 0.99$.⁵

Although we find regular black holes up to $c_1 = 0.99$, we too do not find solutions for $c_1 \geq 1$. There is some evidence that the would-be horizon becomes singular in this case. Indeed, when c_1 approaches 1, the Ricci scalar R and the Kretschmann scalar $K = R^{\alpha\beta\mu\nu} R_{\alpha\beta\mu\nu}$ evaluated on the horizon grow rapidly, as shown in Fig. 1, and at least K_H appears to be diverging, suggesting that no regular black-hole solutions exist when $c_1 = 1$.

Lastly let us note that, as expected, the dimensionless ratio r_g/r_H goes to the GR value (1) when c_1 is small, and decreases for larger c_1 . The deviations away from GR can be very significant as can be seen from Table I, but this is only because the theories under consideration here do not satisfy the constraints of Sec. IV and are therefore allowed to deviate significantly from GR. As we will see in the next section, theories which satisfy all the constraints available to date only allow regular BH solutions that are very similar to the Schwarzschild BHs of GR.

⁵ Our values for γ_{ff} differ significantly from those reported in Ref. [17], but we have determined that the latter were incorrectly computed without accounting for the non-standard normalization of the metric function $F(r)$ at infinity.

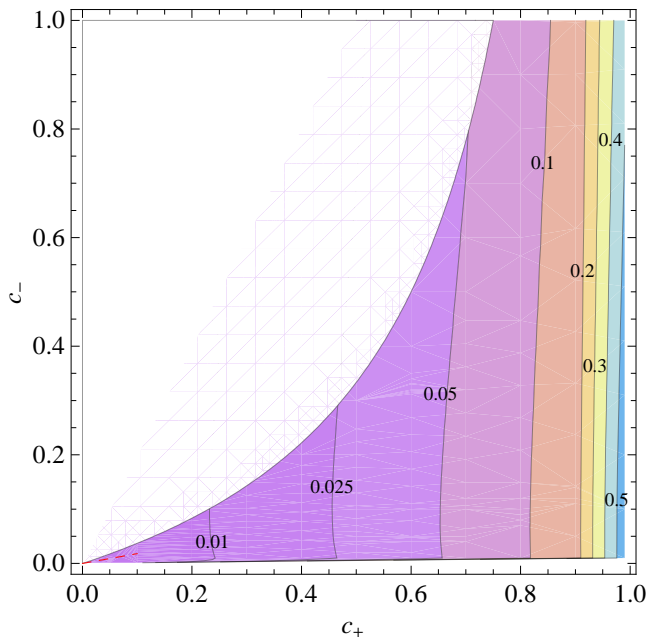


Figure 4: Same as Fig. 2, but for the impact parameter of the circular photon orbit b_{ph} in \mathfrak{a} -theory, normalized against the gravitational radius r_g . Note that the frequency of the circular photon orbit is $\omega_{\text{ph}} = 1/b_{\text{ph}}$.

B. Viable regular BHs in \mathfrak{a} -theory and HL gravity

In this section we focus on the regions of the parameter spaces of \mathfrak{a} -theory and HL gravity that satisfy all the observational constraints available to date, as described in Sec. IV. To this purpose, we have considered 236 points in the parameter plane (c_+, c_-) of \mathfrak{a} -theory and 405 in the parameter plane (β, μ) of HL gravity. Each of these points corresponds to a different gravity theory, and for each of them we have derived the regular asymptotically flat spherical BH solution as described in Sec. III D. To characterize the solutions, we have then extracted, for each of them, the following quantities (explicit expressions for which can be found in the Appendix):

1. The dimensionless product $\omega_{\text{ISCO}} r_g$: ω_{ISCO} is the orbital frequency of the innermost stable circular orbit (ISCO), while r_g is the gravitational radius (54). The deviation of this quantity away from its GR value ($2 \cdot 6^{-3/2}$) is a measure of how easily \mathfrak{a} -theory (or HL gravity) might be discriminated from GR using the X-ray continuum spectra of accretion disks [34, 35] (see also Ref. [36] on how to use these spectra to detect generic deviations from GR black holes) or using future gravitational-wave observations of stellar-mass black holes orbiting around a supermassive black hole (these sources are known as extreme mass-ratio inspirals, or EMRIs) [37].
2. The maximum redshift (measured at spatial infinity) for a photon emitted by a source moving on the ISCO, $z_{\text{max}} = \nu_{\text{emitted}}/\nu_{\text{measured}} - 1$. The maximum

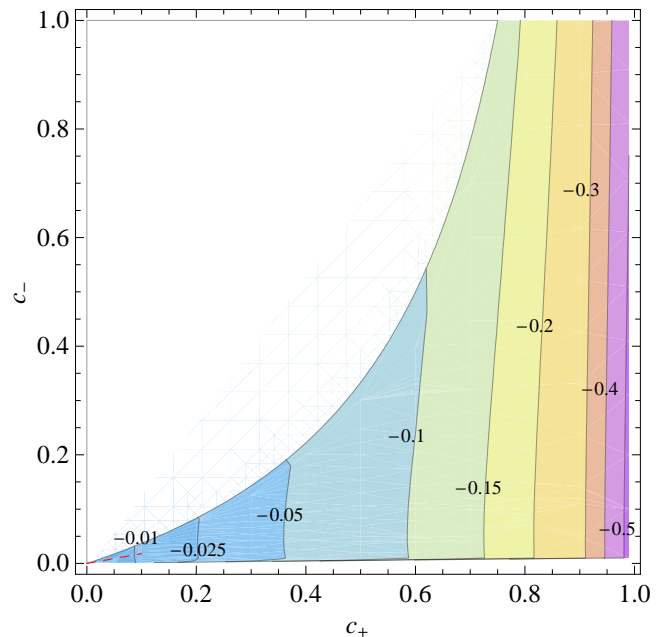


Figure 5: Same as Fig. 2, but for the ratio r_g/r_H of the gravitational radius r_g to the horizon's circumference radius r_H .

redshift comprises both the redshift due to gravitational field of the black hole, and the Doppler redshift, which is maximum for a photon emitted “backward” (*i.e.*, in the negative ϕ direction, if the source moves in the positive ϕ direction). The deviation of this quantity away from its GR value ($3/\sqrt{2} - 1$), together with the value of the combination $\omega_{\text{ISCO}} r_g$ mentioned above, is a measure of how easily a black hole in \mathfrak{a} -theory (or HL gravity) could be distinguished from a Schwarzschild black hole using iron-K α lines [38, 39] (see also Ref. [40] on how to use iron-K α lines to detect deviations from GR black holes).

3. The dimensionless ratio b_{ph}/r_g , where b_{ph} is the impact parameter of the circular photon orbit. The deviations of this quantity from GR (where $b_{\text{ph}}/r_g = 3\sqrt{3}/2$) tell us how easily one can test \mathfrak{a} -theory (or HL gravity) with gravitational lensing experiments (see in particular Ref. [41] for specific attempts to use gravitational lensing to test whether astrophysical black holes are really described by GR). Also, b_{ph} is related to the frequency of the circular photon orbit, $\omega_{\text{ph}} = 1/b_{\text{ph}}$, which in principle will be observable with future gravitational-wave detectors because it regulates the frequency of the black hole gravitational quasi-normal modes, at least in the eikonal approxima-

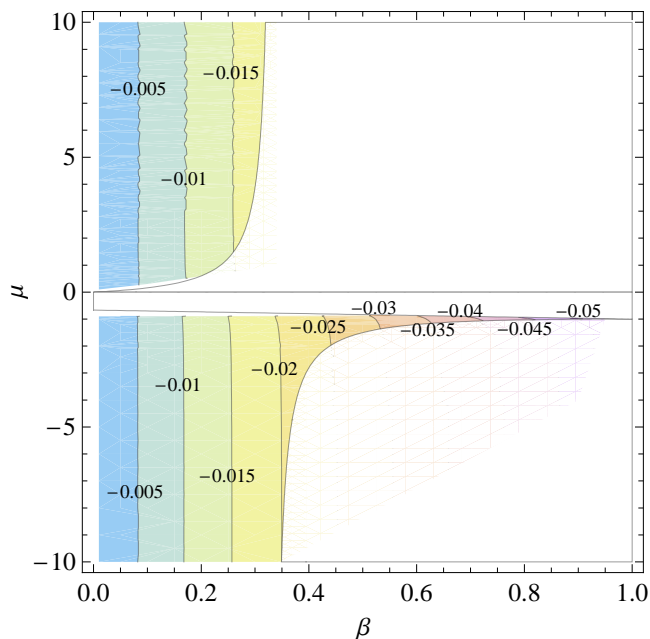


Figure 6: Fractional HL gravity deviation from GR for the dimensionless product $\omega_{\text{ISCO}} r_g$ of the ISCO frequency and the gravitational radius, in the viable region of the parameter plane (see Sec. IV).

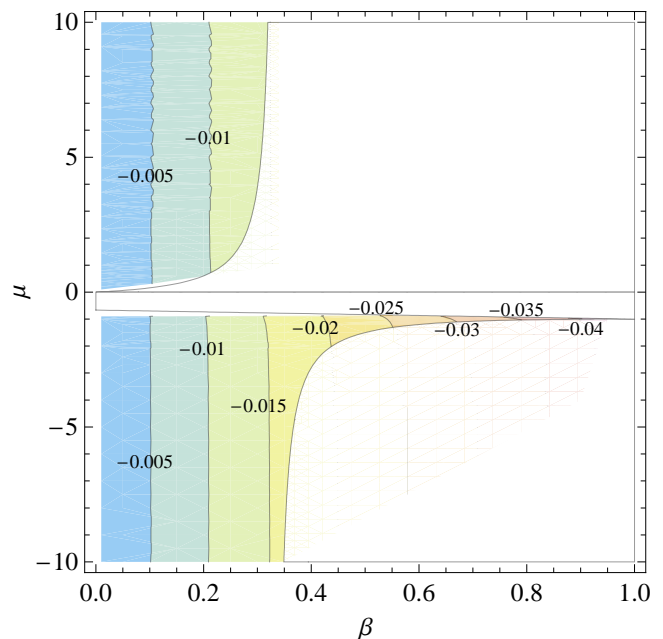


Figure 7: Same as in Fig. 6, but for the maximum redshift of a photon emitted by a source moving on the ISCO, $z_{\text{max}} = \nu_{\text{emitted}}/\nu_{\text{measured}} - 1$. This maximum redshift is obtained for a photon emitted “backward” with respect to the velocity of the source.

tion [42–44].⁶

4. The ratio r_g/r_H . This quantity does not have a direct observational meaning, but we compare it to its GR value (unity) as a way to assess how the near-horizon region of \mathfrak{a} -theory (or HL gravity) differs from GR. This is probably not very important from an observational point of view (because the near-horizon region is hard to observe), but is nevertheless conceptually interesting.

To summarize our results, we have used Mathematica to produce contour plots for the relative deviations of these quantities away from their GR values, as a function of the theory’s parameters — (c_+, c_-) for \mathfrak{a} -theory and (β, μ) for HL gravity. The plots are shown in Figs. 2 to 5 for \mathfrak{a} -theory and in Figs. 6 to 9 for HL gravity. The small wiggles on some of the contours are simply a spurious effect of the numerical procedure used to calculate them.

Two things are striking about these plots. First, the deviations are largely controlled by a single parameter, c_+ in \mathfrak{a} -theory and β in HL gravity. These two parameters are actually the same when the two theories are identified [cf. Eq. (48)]. Second, the contours for the four different quantities in \mathfrak{a} -theory or HL gravity are

very similar. This could be understood if, to a good approximation, the metric function F actually depended on the two coupling parameters only via a single combination. This combination should reduce approximately to c_+ in the \mathfrak{a} -theory case and to β in the HL gravity case to explain the fact that the contours are almost vertical. Using our numerical solutions, we have verified that this is indeed the case. This may seem in contrast with the presence of a term c_{14}/r^3 in the asymptotic metric (24), because the lines $c_{14} = \text{constant}$ are very different from the contours shown in Figs. 2–9. (In the case of \mathfrak{a} -theory, for instance, we have $c_{14} = 2c_+c_-/(c_+ + c_-)$ when the PPN parameters vanish, so the $c_{14} = \text{constant}$ lines are much more horizontal than our contours.) However, we have verified that while the c_{14}/r^3 term is indeed present in our numerical solutions, it is always negligible outside the horizon. This is because that term is suppressed by a factor $1/48$ [cf. Eq. (24)] and because $|c_{14}| \lesssim 2$ in the part of parameter space that we explore, both in \mathfrak{a} -theory and HL gravity. Higher order terms in the $1/r$ expansion are, however, important, and are responsible for producing the deviations from GR in the dimensionless quantities plotted in the figures (the deviation of r_g/r_H from its GR value is also sensitive to the $1/r$ term).

As can be seen, the deviations from GR are quite small. In \mathfrak{a} -theory, they do not reach the 10% level until $c_+ \approx 0.7$, while in HL gravity they remain less than 3% in most of the parameter space. Such small deviations are probably undetectable with accretion disk spectra, iron-K α lines, or gravitational lensing, at least with

⁶ Quasi-normal modes of black hole solutions in \mathfrak{a} -theory were studied in Refs. [45, 46] under the assumption that the aether remains unperturbed.

present data. The only exception might be the region $0.9 < c_+ < 1$ in the \mathfrak{a} -theory parameter plane, where the deviations from GR are larger than 20% and might therefore be observable with these techniques, provided that systematic errors in the data and astrophysical uncertainties are properly understood. However, this region is presumably already ruled out by observations of gravitational radiation damping from binary pulsars [32].

The size of the black hole modifications we have found is comparable to the effects on neutron star structure reported in Ref. [47]. (The solution outside a star, in which the aether is aligned with the timelike Killing vector, is different from the black hole solution, in which the aether flows inward.) There the maximum mass, surface redshift, and ISCO frequency were computed for various equations of state. Depending on the equation of state, the maximum masses are about 6% - 15% smaller than in GR when the \mathfrak{a} -theory parameter c_{14} is equal to 1, and the corresponding surface redshifts are roughly 10% larger than in GR. The ISCO frequency, which is independent of the equation of state, is only 4% smaller than in GR. Thus, it also appears challenging to obtain useful constraints from neutron star observations.

On the other hand, future gravitational-wave experiments such as LISA will be able to test deviations from the Kerr metric with astonishing accuracy ($\sim 10^{-6}$) using extreme mass-ratio inspirals (EMRIs) [37]. While further work is necessary to be ready to use LISA data for testing \mathfrak{a} -theory or HL gravity, such an accuracy is more than enough (by orders of magnitude) to detect the deviations of \mathfrak{a} -theory (HL gravity) from GR predicted by our code, essentially in all of the parameter space. Observations of EMRIs with LISA could, therefore, allow very strong constraints to be put on \mathfrak{a} -theory and HL gravity.

C. The interior solutions

In LV theories different modes generically propagate at different velocities. Additionally, they no longer necessarily satisfy linear dispersion relations, which means that the limiting speed of short wavelength disturbances can be infinite in the preferred frame. Indeed \mathfrak{a} -theory has the first of these characteristics and (full) HL gravity has both of them, as we will discuss in more detail below. In such theories a mode can potentially escape the horizon defined by another mode, or there might not be any horizons at all. It is therefore potentially of observational interest to study the interior behavior of the black hole solutions. It is also in any case of mathematical and fundamental interest. We present here some results for this behavior.

In general, irrespective of the parameters (c_+, c_-) or (β, μ) of the theory, the solutions that we have found always present a spacelike curvature singularity at $r = 0$, where the Ricci scalar R and the Kretschmann scalar $R_{\alpha\beta\mu\nu}R^{\alpha\beta\mu\nu}$ (as well as the metric function F) diverge.

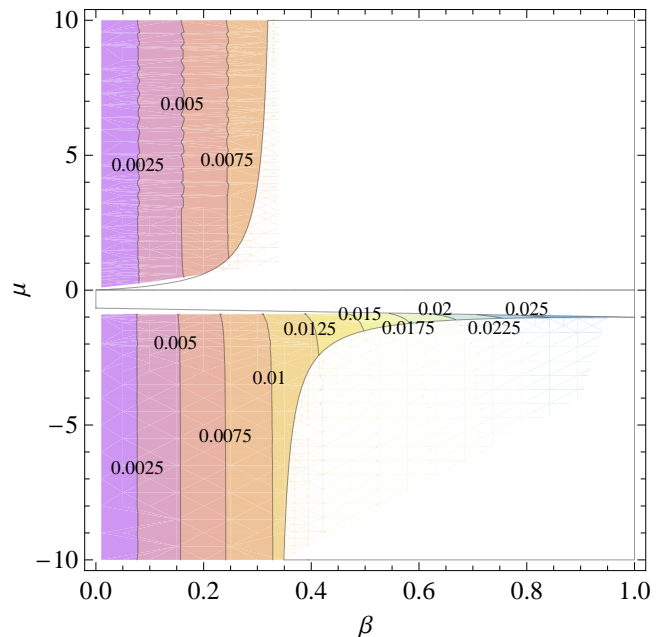


Figure 8: Same as in Fig. 6, but for the impact parameter of the circular photon orbit b_{ph} , normalized against the gravitational radius r_g . Note that the frequency of the circular photon orbit is $\Omega_{\text{ph}} = 1/b_{\text{ph}}$.

The aether, to the contrary, presents an oscillatory behavior, as already noticed in Ref. [17]. To see this, we have studied the Lorentz factor $\gamma_r \equiv u_{\text{obs}}^\alpha u_\alpha$ of the aether as measured by the future directed observer orthogonal to the (spacelike) hypersurface $r = \text{constant}$. In Figs. 10-12 we plot the corresponding boost angle

$$\theta_r = \text{arccosh} \gamma_r, \quad (55)$$

for three representative cases,⁷ as a function of r (which plays the role of a time coordinate inside the horizon).

For the case in Fig. 10 (\mathfrak{a} -theory with $c_- = 0.0018$, $c_+ = 0.01$), after an initial transient, the boost angle oscillates with roughly constant amplitude, and roughly constant period when measured in terms of $\log r$, thus corresponding to an undamped oscillator. The case shown in Fig. 11 (\mathfrak{a} -theory with $c_+ = 0.99$, $c_- = 0.01$) resembles instead a damped oscillator, while the case shown in Fig. 12 (HL gravity with $\beta = 0.4$, $\mu = -1.8$) resembles, after an initial transient, an over-damped oscillator (*i.e.* one in which the damping is so strong that it does not oscillate, but approaches the rest position exponentially).

This oscillatory behavior is reminiscent of that found for the aether in (anisotropic) Bianchi type I (Kasner-

⁷ These cases seem qualitatively representative of the inner solutions of all of the regular black holes that we studied, although we have not yet performed a full parameter space scan like those presented in the previous section.

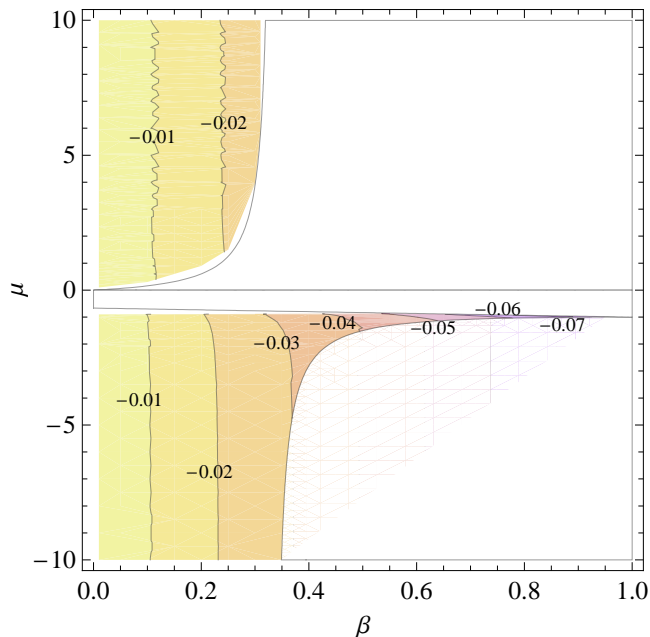


Figure 9: Same as in Fig. 6, but for the ratio r_g/r_H of the gravitational radius r_g to the horizon’s circumference radius r_H .

like) cosmologies with a cosmological constant, both in HL and \mathfrak{a} -theory [48]. This analogy is understandable, since the black hole interior also corresponds to an anisotropic cosmology, although of a different symmetry type and spatial curvature, and without a cosmological constant. As remarked in Ref. [17], it is also reminiscent of oscillations found in the interior of Einstein-Yang-Mills black hole solutions [49]. Presumably the appearance of oscillations can be understood from the cosmological point of view as an attractor arising because of a “restoring force” that tends to align the cosmological rest frame with any other preferred frame defined by the other (non-metric) fields.

There is an important causal implication of these oscillations, namely, they imply that the concept of a black hole survives in these theories, as we now explain [50]. In \mathfrak{a} -theory, the spin-0, spin-1, and spin-2 perturbations generally all travel at different speeds, and we have assumed they are all greater than or equal to the metric speed of light in order to satisfy the vacuum Čerenkov constraints. Such perturbations could therefore escape from a metric horizon, although they might have deeper causal horizons trapping them. The same will hold for the spin-0 and spin-2 perturbations in the low energy limit of HL gravity. However, the situation is quite different when the full HL theory is considered, *i.e.* when the higher order terms in L_4 and L_6 (and presumably the corresponding higher order spatial derivative terms for matter fields) are also taken into account. Because these terms contain higher spatial derivatives, short wavelength perturbations can travel at arbitrarily high speed relative to the aether. This raises the possi-

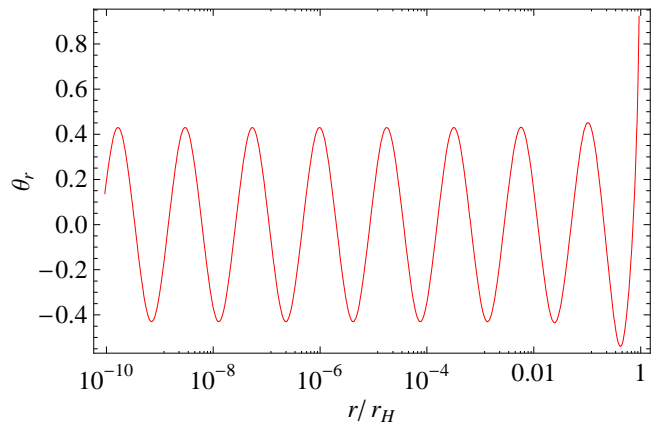


Figure 10: The aether’s boost angle $\theta_r = \text{arccosh}\gamma_r$ with respect to the future-directed observer orthogonal to the hypersurfaces $r = \text{const}$, as a function of radius and inside the metric horizon ($r = r_H$). This is for \mathfrak{a} -theory with $c_- = 0.0018$, $c_+ = 0.01$.

bility that in HL gravity signals can always escape from *anywhere* inside a black hole, in which case the concept of black hole really would not survive at all in HL gravity.

However, even at infinite speed, signals cannot travel backward in time, *i.e.* backward across the constant T hypersurfaces which are orthogonal to the aether (9). These hypersurfaces define a universal causal structure in HL gravity, and in hypersurface-orthogonal aether configurations. When the boost angle (55) vanishes, the aether is orthogonal to a constant- r hypersurface $r = r_c$, which therefore coincides with a constant- T hypersurface. Events at $r < r_c$ (which lie to the future of r_c) therefore can have no influence on events at $r > r_c$, so signals are trapped within the radius r_c [50]. In fact the oscillatory behavior means that there are many such surfaces inside the black hole. In the examples shown in Figs. 10-12, the first such surface occurs quite close to the metric horizon, as measured by r . We refer to the outermost such surface as the “universal horizon”.

The HL time function T therefore has a peculiar behavior in the black hole interior. A surface of constant T that comes in from spatial infinity crosses the metric horizon smoothly, but then, unlike the familiar Painlevé-Gullstrand time coordinate, rather than running into the singularity at $r = 0$ this surface dips down to the infinite past, measured in the advanced time coordinate v , at the universal horizon. This behavior of T happens despite the fact that the aether vector and the geometry are perfectly smooth all the way up to the singularity. To understand what is happening, we note that spherical and time translation symmetry imply that T has the form $T(v, r) = h(v + f(r))$, where $f(r)$ is determined by the metric and aether, and the function h is completely arbitrary (other than that it be monotonic) on account of the T -reparametrization symmetry of the theory, Eq. (16). It turns out that the function $f(r)$ diverges at the

VI. CONCLUSIONS

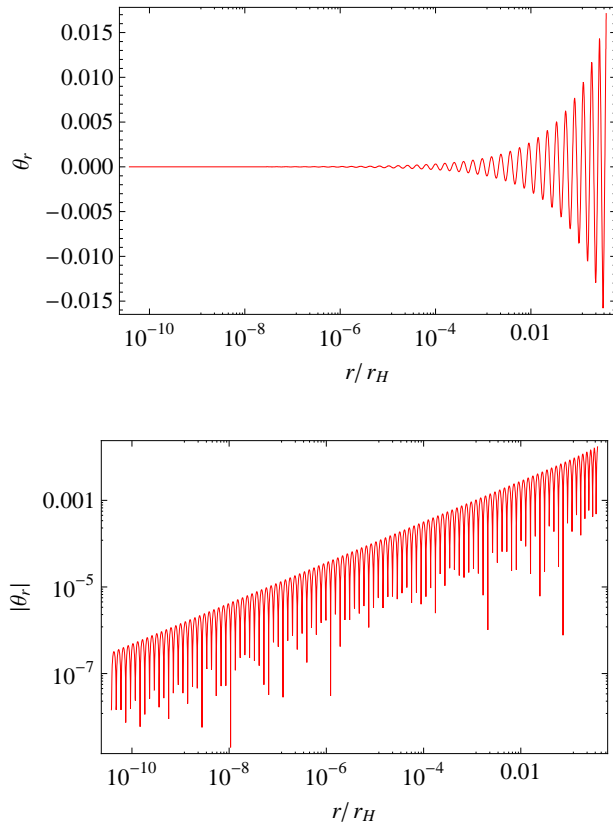


Figure 11: The same as in Fig. 10, but for æ-theory with $c_+ = 0.99$, $c_- = 0.01$.

universal horizon (and at the similar surfaces inside it). Thus, on a constant T surface, $v \rightarrow -\infty$ as the universal horizon is approached. Also, on an ingoing light ray at constant v , the function T diverges unless h is chosen properly. For instance, we could choose h to be minus the inverse of f , in which case T remains finite and increasing when approaching the universal horizon from the outside at constant v .

A final important comment is that the solutions we have been discussing apply only in the IR limit of HL gravity, *i.e.* they neglect the effects of higher derivative terms in the HL action (17). Those terms will certainly strongly affect the solution in the black hole interior where the curvature becomes large. However, as remarked above, the universal horizon appears fairly close to the metric horizon, in a region where one would expect the IR limit of the theory to still be an excellent approximation for macroscopic black holes. Hence, there is good reason to expect that sufficiently large black holes in the full HL theory also possess a universal horizon.

We have studied static, spherically symmetric, black-hole solutions in Einstein-aether theory. These are also solutions of the low-energy limit of Hořava–Lifshitz gravity. We highlight below the most important steps in the process of finding these solutions (setting aside technical issues) and summarize their salient properties.

In general these spacetimes have both a metric horizon and a horizon for the spin-0 mode of the aether, as the latter travels at different speed than the speed of light defined by the metric cone. The vacuum Čerenkov constraint requires that the speed of the spin-0 mode be greater than or equal to the speed of light, so we only considered cases where the spin-0 horizon lies inside the metric horizon. Additionally, we have imposed the condition that the spin-0 horizon be regular, as this is what is expected for black holes that form from gravitational collapse.

Imposing this regularity condition and the condition of asymptotic flatness leads to a one parameter family of solutions for each set of the parameters of the theory. In units where the horizon radius is 1 this yields a unique solution for that set of theory parameters. We have generated this solution numerically. A crucial step towards this has been the realization that a specific combination of the field equations constitutes a set of constraint equations. Additionally, a suitable field redefinition has been utilized in order to facilitate imposition of the condition of regularity at the spin-0 horizon.

We have restricted attention to the regions of the parameter space, both in Einstein-aether theory and Hořava–Lifshitz gravity, where the following conditions are satisfied: (i) stability and positive energy of all perturbations; (ii) avoidance of vacuum Čerenkov radiation; (iii) exact agreement with the first post-Newtonian predictions of GR (vanishing preferred frame parameters). (The regions of the parameter space where these conditions are satisfied do not coincide for the two theories.)

We find that regular, asymptotically flat black-hole solutions exist in all of the explored parameter regions satisfying these observational constraints. In order to characterize the solutions, we used three dimensionless quantities that are in principle measurable by observations: the product of the orbital frequency of the Innermost Stable Circular Orbit (ISCO) with the gravitational radius, the maximum redshift of a photon emitted by a source moving on the ISCO, and the ratio between the impact parameter of the circular photon orbit and the gravitational radius. As a fourth probe we used the ratio between the gravitational radius and the horizon radius.

The deviations of these quantities from the values that they have in general relativity are always quite small, exceeding 10% (in Einstein-aether theory) and 3% (in Hořava–Lifshitz gravity) only in restricted portions of the parameter space. Therefore, they are expected to be difficult, although perhaps not impossible, to detect by electromagnetic observations such as accretion disk

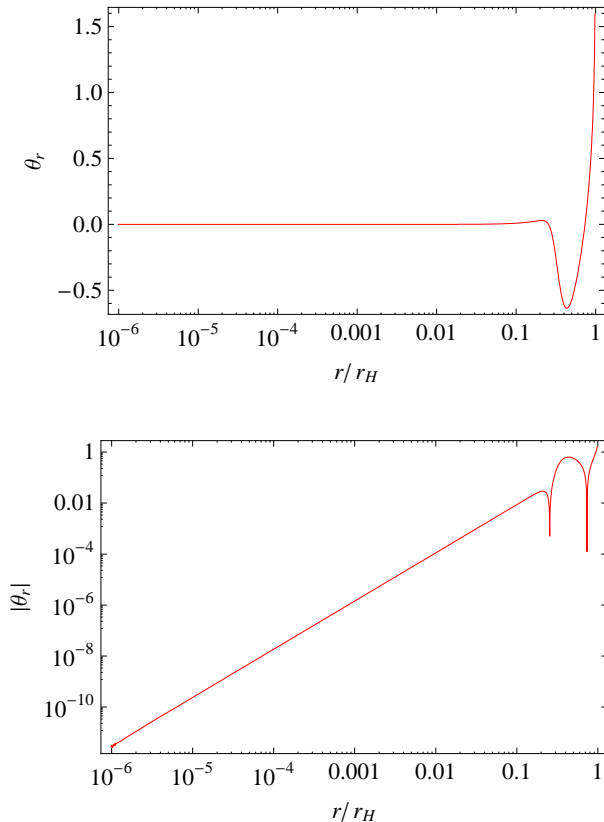


Figure 12: The same as in Fig. 10, but for HL gravity with $\beta = 0.4$, $\mu = -1.8$.

spectra, iron-K α lines or gravitational lensing. However, future gravitational-wave experiments, such as LISA, would have more than sufficient accuracy to detect these deviations from general relativity.

Last but not least, we considered the interior solution. Inside the black hole the aether oscillates with respect to the constant r surfaces, and there is a spacelike singularity at $r = 0$. More importantly, it turns out that there exists a universal horizon inside the metric and spin-0 horizons, *i.e.* a surface of constant r that is orthogonal to the aether. No modes can escape from inside the universal horizon, even those satisfying modified dispersion relations that could allow them to travel at arbitrarily high speeds relative to the aether, as expected in Hořava–Lifshitz gravity. The existence of this universal horizon implies that the concept of a black hole, in the sense of a region of spacetime where all signals are trapped, seems to survive in these theories.

Acknowledgments

E.B. acknowledges support from NSF Grant PHY-0903631. TJ was supported in part by the NSF under grant PHY-0903572. TPS was supported by a Marie Curie Fellowship.

Appendix: Quantities used to characterize the solutions

The innermost stable circular orbit (ISCO) occurs at the radius $r = r_{\text{ISCO}}$ where

$$-2rF'^2 + F(3F' + rF'') = 0. \quad (\text{A.1})$$

The ISCO frequency is

$$\omega_{\text{ISCO}} = \sqrt{\frac{F'}{2r}} \Big|_{\text{ISCO}}. \quad (\text{A.2})$$

The redshift $z = \nu_0/\nu_\infty - 1$ of a photon emitted by a source orbiting at the ISCO and measured at infinity is given by

$$1 + z = \frac{1 - \omega b}{\sqrt{F - \omega^2 r^2}} \Big|_{\text{ISCO}}, \quad (\text{A.3})$$

where b is the impact parameter of the photon, which is defined as its angular momentum divided by its energy, and which characterizes the direction of emission. For instance, for a photon transverse to the orbit one has $b = 0$, while for photons emitted in the forward or backward directions one has $b = \pm(r/\sqrt{F})_{\text{ISCO}}$. The maximum redshift z_{max} is therefore in the backward direction,

$$1 + z_{\text{max}} = \frac{1 + \omega r F^{-1/2}}{\sqrt{F - \omega^2 r^2}} \Big|_{\text{ISCO}}, \quad (\text{A.4})$$

and this is because the Doppler shift is maximized in this case.

The circular photon orbit occurs at $r = r_{\text{ph}}$, where

$$-2F + rF' = 0. \quad (\text{A.5})$$

The impact parameter of the photon orbit is given by

$$b_{\text{ph}} = \frac{r}{\sqrt{F}} \Big|_{\text{ph}}, \quad (\text{A.6})$$

while its frequency is $\omega_{\text{ph}} = 1/b_{\text{ph}}$.

The relative Lorentz gamma factor between the aether and the unit Killing energy observer at the horizon, which corresponds to an observer that falls in radially from rest at infinity, is

$$\gamma_{\text{H}} = u_\mu u_{\text{H}}^\mu = A_{\text{H}} + \frac{1}{4A_{\text{H}}}, \quad (\text{A.7})$$

when the v coordinate is normalized so that $F_\infty = 1$. The relative gamma factor between the aether and the unit (timelike) normal to the constant r surfaces inside the metric horizon is

$$\gamma_r = -\frac{u^r}{\sqrt{g^{rr}}} \quad (\text{A.8})$$

from which we define the boost angle as $\theta_r = \text{arccosh}(\gamma_r)$.

-
- [1] D. Mattingly, “Modern tests of Lorentz invariance,” *Living Rev. Rel.* **8** (2005) 5 [arXiv:gr-qc/0502097].
- [2] S. Liberati and L. Maccione, “Lorentz Violation: Motivation and new constraints,” *Ann. Rev. Nucl. Part. Sci.* **59** (2009) 245 [arXiv:0906.0681 [astro-ph.HE]].
- [3] See, for example, M. Gasperini, “Singularity prevention and broken Lorentz symmetry,” *Class. Quantum Grav.* **4**, (1987) 485; “Repulsive gravity in the very early Universe,” *Gen. Rel. Grav.* **30** (1998) 1703; and references therein.
- [4] T. Jacobson and D. Mattingly, “Gravity with a dynamical preferred frame,” *Phys. Rev. D* **64**, 024028 (2001) [arXiv:gr-qc/0007031].
- [5] T. Jacobson, “Einstein-aether gravity: a status report,” *PoS QG-PH*, 020 (2007) [arXiv:0801.1547].
- [6] B. Withers, *Class. Quant. Grav.* **26**, 225009 (2009). [arXiv:0905.2446 [gr-qc]].
- [7] P. Horava, “Quantum Gravity at a Lifshitz Point,” *Phys. Rev. D* **79**, 084008 (2009). [arXiv:0901.3775 [hep-th]].
- [8] C. Charmousis, G. Niz, A. Padilla and P. M. Saffin, “Strong coupling in Horava gravity,” *JHEP* **0908**, 070 (2009) [arXiv:0905.2579]; M. Li and Y. Pang, “A Trouble with Hořava-Lifshitz Gravity,” *JHEP* **0908**, 015 (2009) [arXiv:0905.2751]; A. A. Kocharyan, “Is nonrelativistic gravity possible?,” *Phys. Rev. D* **80**, 024026 (2009) [arXiv:0905.4204]; D. Blas, O. Pujolas and S. Sibiryakov, “On the Extra Mode and Inconsistency of Horava Gravity,” *JHEP* **0910**, 029 (2009) [arXiv:0906.3046]; A. Wang and R. Maartens, “Linear perturbations of cosmological models in the Horava-Lifshitz theory of gravity without detailed balance,” *Phys. Rev. D* **81**, 024009 (2010) [arXiv:0907.1748]; N. Afshordi, “Cuscuton and low energy limit of Horava-Lifshitz gravity,” *Phys. Rev. D* **80**, 081502(R) (2009) [arXiv:0907.5201]; K. Koyama and F. Arroja, “Pathological behaviour of the scalar graviton in Hořava-Lifshitz JHEP **1003**, 061 (2010) [arXiv:0910.1998]; M. Henneaux, A. Kleinschmidt and G. L. Gomez, “A dynamical inconsistency of Horava gravity,” *Phys. Rev. D* **81**, 064002 (2010) [arXiv:0912.0399].
- [9] T. P. Sotiriou, M. Visser and S. Weinfurter, *Phys. Rev. Lett.* **102**, 251601 (2009) [arXiv:0904.4464 [hep-th]]; “Quantum gravity without Lorentz invariance,” *JHEP* **0910**, 033 (2009) [arXiv:0905.2798];
- [10] D. Blas, O. Pujolas and S. Sibiryakov, “Consistent Extension Of Horava Gravity,” *Phys. Rev. Lett.* **104**, 181302 (2010) [arXiv:0909.3525].
- [11] A. Papazoglou and T. P. Sotiriou, “Strong coupling in extended Horava-Lifshitz gravity,” *Phys. Lett. B* **685**, 197 (2010) [arXiv:0911.1299 [hep-th]].
- [12] I. Kimpton and A. Padilla, “Lessons from the decoupling limit of Horava gravity,” *JHEP* **1007**, 014 (2010) [arXiv:1003.5666 [Unknown]].
- [13] D. Blas, O. Pujolas and S. Sibiryakov, “Comment on ‘Strong coupling in extended Horava-Lifshitz gravity’,” *Phys. Lett. B* **688**, 350 (2010) [arXiv:0912.0550 [hep-th]].
- [14] C. Germani, A. Kehagias and K. Sfetsos, “Relativistic Quantum Gravity at a Lifshitz Point,” *JHEP* **0909**, 060 (2009) [arXiv:0906.1201 [hep-th]].
- [15] T. Jacobson, “Extended Horava gravity and Einstein-aether theory,” arXiv:1001.4823 [gr-qc].
- [16] D. Blas, O. Pujolas, S. Sibiryakov, “Models of non-relativistic quantum gravity: The Good, the bad and the healthy,” [arXiv:1007.3503 [hep-th]].
- [17] C. Eling and T. Jacobson, “Black holes in Einstein-aether theory,” *Class. Quant. Grav.* **23**, 5643 (2006) [arXiv:gr-qc/0604088].
- [18] T. Tamaki, U. Miyamoto, “Generic features of Einstein-Aether black holes,” *Phys. Rev. D* **77**, 024026 (2008). [arXiv:0709.1011 [gr-qc]].
- [19] J. Greenwald, A. Papazoglou and A. Wang, “Black holes and stars in Horava-Lifshitz theory with projectability condition,” *Phys. Rev. D* **81**, 084046 (2010) [arXiv:0912.0011 [hep-th]].
- [20] H. Lu, J. Mei and C. N. Pope, “Solutions to Horava Gravity,” *Phys. Rev. Lett.* **103**, 091301 (2009) [arXiv:0904.1595 [hep-th]].
- [21] A. Kehagias and K. Sfetsos, “The black hole and FRW geometries of non-relativistic gravity,” *Phys. Lett. B* **678**, 123 (2009) [arXiv:0905.0477 [hep-th]].
- [22] E. Kiritsis and G. Kofinas, “On Horava-Lifshitz ‘Black Holes’,” *JHEP* **1001**, 122 (2010) [arXiv:0910.5487 [hep-th]].
- [23] E. Kiritsis, “Spherically symmetric solutions in modified Horava-Lifshitz gravity,” *Phys. Rev. D* **81**, 044009 (2010) [arXiv:0911.3164 [hep-th]].
- [24] C. Eling and T. Jacobson, “Spherical Solutions in Einstein-Aether Theory: Static Aether and Stars,” *Class. Quant. Grav.* **23**, 5625 (2006) [arXiv:gr-qc/0603058].
- [25] S. M. Carroll and E. A. Lim, “Lorentz-violating vector fields slow the universe down,” *Phys. Rev. D* **70**, 123525 (2004) [arXiv:hep-th/0407149].
- [26] T. Jacobson and D. Mattingly, “Einstein-aether waves,” *Phys. Rev. D* **70**, 024003 (2004) [arXiv:gr-qc/0402005].
- [27] B. Z. Foster, “Metric redefinitions in Einstein-aether theory,” *Phys. Rev. D* **72**, 044017 (2005) [arXiv:gr-qc/0502066].
- [28] J. W. Elliott, G. D. Moore, H. Stoica, “Constraining the new Aether: Gravitational Cerenkov radiation,” *JHEP* **0508**, 066 (2005). [hep-ph/0505211].
- [29] D. Garfinkle, C. Eling and T. Jacobson, “Numerical simulations of gravitational collapse in Einstein-aether theory,” *Phys. Rev. D* **76**, 024003 (2007) [arXiv:gr-qc/0703093].
- [30] C. Eling and T. Jacobson, “Static post-Newtonian equivalence of GR and gravity with a dynamical preferred frame,” *Phys. Rev. D* **69**, 064005 (2004) [arXiv:gr-qc/0310044].
- [31] C. M. Will, “The confrontation between general relativity and experiment,” *Living Rev. Rel.* **9**, 3 (2005) [arXiv:gr-qc/0510072].
- [32] B. Z. Foster, “Strong field effects on binary systems in Einstein-aether theory,” *Phys. Rev. D* **76**, 084033 (2007) [arXiv:0706.0704 [gr-qc]].
- [33] B. Z. Foster, “Radiation Damping in Einstein-Aether Theory,” *Phys. Rev. D* **73**, 104012 (2006) [Erratum-ibid. **D 75**, 129904 (2007)] [arXiv:gr-qc/0602004].
- [34] S. N. Zhang, W. Cui and W. Chen 1997, *Astrophys. J.* **482**, L155 (1997).
- [35] J. E. McClintock *et al.*, “Measuring the Spins of Accreting Black Holes,” arXiv:1101.0811 [astro-ph.HE].

- [36] C. Bambi, E. Barausse, “Constraining the quadrupole moment of stellar-mass black-hole candidates with the continuum fitting method,” [arXiv:1012.2007 [gr-qc]].
- [37] P. Amaro-Seoane, J. R. Gair, M. Freitag *et al.*, “Astrophysics, detection and science applications of intermediate- and extreme mass-ratio inspirals,” *Class. Quant. Grav.* **24**, R113-R169 (2007).
- [38] A. C. Fabian, M. J. Rees, L. Stella *et al.*, “X-ray fluorescence from the inner disc in Cygnus X-1,” *Mon. Not. Roy. Astron. Soc.* **238**, 729-736 (1989).
- [39] C. S. Reynolds, M. A. Nowak, “Fluorescent iron lines as a probe of astrophysical black hole systems,” *Phys. Rept.* **377**, 389-466 (2003)
- [40] D. Psaltis and T. Johannsen, “A Ray-Tracing Algorithm for Spinning Compact Object Spacetimes with Arbitrary Quadrupole Moments. I. Quasi-Kerr Black Holes,” arXiv:1011.4078 [astro-ph.HE].
- [41] T. Johannsen and D. Psaltis, “Testing the No-Hair Theorem with Observations in the Electromagnetic Spectrum: II. Black-Hole Images,” *Astrophys. J.* **718**, 446 (2010)
- [42] B. Mashhoon, *Phys. Rev. D* **31**, 290 (1985).
- [43] V. Cardoso, A. S. Miranda, E. Berti *et al.*, “Geodesic stability, Lyapunov exponents and quasinormal modes,” *Phys. Rev.* **D79**, 064016 (2009).
- [44] S. Hod, “Black-hole quasinormal resonances: Wave analysis versus a geometric-optics approximation,” *Phys. Rev.* **D80**, 064004 (2009). [arXiv:0909.0314 [gr-qc]].
- [45] R. A. Konoplya and A. Zhidenko, “Perturbations and quasi-normal modes of black holes in Einstein-Aether theory,” *Phys. Lett. B* **644**, 186 (2007) [arXiv:gr-qc/0605082].
- [46] R. A. Konoplya and A. Zhidenko, “Gravitational spectrum of black holes in the Einstein-Aether theory,” *Phys. Lett. B* **648**, 236 (2007) [arXiv:hep-th/0611226].
- [47] C. Eling, T. Jacobson and M. C. Miller, “Neutron stars in Einstein-aether theory,” *Phys. Rev. D* **76**, 042003 (2007) [Erratum-ibid. *D* **80**, 129906 (2009)] [arXiv:0705.1565 [gr-qc]].
- [48] I. Carruthers, T. Jacobson, “Cosmic alignment of the aether,” *Phys. Rev.* **D83**, 024034 (2011). [arXiv:1011.6466 [gr-qc]].
- [49] E. E. Donets, D. V. Galtsov, M. Y. Zotov, “Internal structure of Einstein Yang-Mills black holes,” *Phys. Rev.* **D56**, 3459-3465 (1997). [gr-qc/9612067].
- [50] This point was made in a talk by Sergey Sibiriyakov at the Peyresq 15 meeting, June, 2010.